

Elastic Locomotion with Mixed Second-order Differentiation

SIYUAN SHEN, TIANJIA SHAO, and KUN ZHOU, State Key Laboratory of CAD&CG, Zhejiang University, China
CHENFANFU JIANG, UCLA, USA

SHELDON ANDREWS, École de technologie supérieure (ÉTS), Canada and Roblox, USA

VICTOR ZORDAN, Roblox, USA

YIN YANG*, University of Utah, USA



Fig. 1. A gymnast lamp. Elastic locomotion offers the user a convenient way to bring elastic bodies to life. By specifying intuitive and high-level motion descriptions, our framework finds the optimal muscle activations that drive the body to achieve those kinematic targets. The key to solve this problem is a mixed second-order differentiation that augments reverse automatic differentiation with complex-step finite differences. This allows the Hessian of a user-defined loss function to be conveniently evaluated. In this teaser example, a lamp first jumps onto a small stool, then onto a higher glass table (they have different surface frictions), performs a flip and twist in mid-air, and finally lands on the ground. It takes about 20 sec to optimize each time step ($\Delta t = 1/40$ sec), and we only need two Newton iterations on average to solve the inverse problem. This is not possible with existing first-order methods.

We present a framework of elastic locomotion, which allows users to enliven an elastic body to produce interesting locomotion by prescribing its high-level kinematics. We formulate this problem as an inverse simulation problem and seek the optimal muscle activations to drive the body to complete the desired actions. We employ the interior-point method to model wide-area contacts between the body and the environment with logarithmic barrier penalties. The core of our framework is a mixed second-order differentiation algorithm. By combining both analytic differentiation and numerical differentiation modalities, a general-purpose second-order differentiation scheme is made possible. Specifically, we augment complex-step finite difference (CSFD) with reverse automatic differentiation (AD). We treat AD as a generic function, mapping a computing procedure to its derivative w.r.t. output loss, and promote CSFD along the AD computation. To this end, we carefully implement all the arithmetics used in elastic locomotion, from elementary functions to linear algebra and matrix operation for CSFD promotion. With this novel differentiation tool, elastic locomotion can directly exploit Newton's method and use its strong second-order convergence to

*Corresponding author.

Authors' addresses: Siyuan Shen, messyshen@gmail.com; Tianjia Shao, tjshao@zju.edu.cn; Kun Zhou, kunzhou@acm.org, State Key Laboratory of CAD&CG, Zhejiang University, Hangzhou, China; Chenfanfu Jiang, UCLA, Los Angeles, USA, chenfanfu.jiang@gmail.com; Sheldon Andrews, École de technologie supérieure (ÉTS), Montreal, Canada and Roblox, San Mateo, USA, sheldon.andrews@etsmtl.net; Victor Zordan, Roblox, San Mateo, USA, vbzordan@roblox.com; Yin Yang, University of Utah, Salt Lake City, USA, yangzzzy@gmail.com.

find the needed activations at muscle fibers. This is not possible with existing first-order inverse or differentiable simulation techniques. We showcase a wide range of interesting locomotions of soft bodies and creatures to validate our method.

Additional Key Words and Phrases: Elastodynamics, Locomotion control, Differentiation, Optimization

1 INTRODUCTION

The animation of deformable characters is a desirable goal for bringing real-world and fantastic characters to life. While many characters rely on an underlying piece-wise rigid skeleton rig to achieve coordinated motions, there are also a lot of creatures that do not have embedded bones – they exploit muscular actuators to contract or expand parts of the body to enable unique and vibrant interactions with the environment. Unlike a skeleton rig, a soft body has a flexible and extensive surface, leading to wide contacting areas with the environment e.g., the ground. As a result, calculating a good locomotion control of the soft body inevitably needs to deal with a high-dimension contact problem involving a set of inequality constraints. While the mathematical model of contact has been well-studied, e.g., one can simplify it to linear complementarity programming [Cottle et al. 2009], it is known NP-Hard [Chung

1989] due to its combinational nature and remains computationally challenging in practice.

Most real-world materials are nonlinear. Forward simulation of a soft body by specifying external forces is already expensive as tens of thousands of unknown degrees of freedom (DOFs) are two-way coupled. It becomes tricky if the user wants direct and intuitive control over the result of the simulation, e.g., to have movement of the body to follow a prescribed path. This is because the objective function and the control parameters are implicitly related by the forward process without a closed-form mathematical expression, and this implicit relation also involves a set of contact constraints. Such combined high nonlinearity and high dimensionality are beyond the capability of the existing simulation techniques, making the problem of elastic locomotion particularly challenging.

We develop a framework that enables an intuitive control of an elastic body's locomotion. The user directs the motion, pose, or trajectory of the body via high-level and straightforward kinetic descriptors, and our algorithm inversely estimates the optimal muscle activations to achieve the desired dynamic state at the next frame. We are inspired by incremental potential contact or IPC [Li et al. 2020]. IPC re-formulates inequality constraints using logarithmic barrier penalties and converts the contact problem to an unconstrained optimization. This strategy allows us to tackle higher-dimensional contact instances since IPC obviates the combinational optimization inherent in the complementarity programming. On the downside, IPC further escalates the nonlinearity of the forward simulation. The resulting optimization is bumpy and irregular and has a large number of saddle points and local minima. Existing differentiable or inverse simulation techniques, which are primarily based on gradient information of the loss function are barely helpful.

This paper proposes a novel mixed differentiation modality that allows an efficient evaluation of second-order differentiation for elastic locomotion so that we can use high-order optimization tools like Newton's method to overcome the nonlinearity induced by inverse elastodynamics and IPC barriers. The core idea is to combine analytic differentiation of auto differentiation (AD) [Bartholomew-Biggs et al. 2000; Corliss et al. 2013], which generates a programming procedure of the analytic differentiation of a function, with numerical differentiation, which estimates the differentiation of a function without knowing its closed-form. Specifically, we employ complex-step finite difference (CSFD) [Luo et al. 2019; Shen et al. 2021] as our numerical differentiation method and augment CSFD with reverse AD. Compared with other numerical differentiation methods such as finite difference, CSFD has several favored properties. First, CSFD is numerically stable and accurate. It does not have the subtractive cancellation issue, so one can choose a sufficiently small perturbation size to fully suppress the approximation error, making CSFD as accurate as the analytic result. There are many off-the-shelf complex libraries. Thus, we do not need to build our differentiation method from scratch.

2 RELATED WORK

In this section, we briefly discuss some prior contributions relevant to soft body control, trajectory optimization, and differentiation.

2.1 Soft body Control

The appeal of animated soft body controllers has led to the introduction a number of techniques offering solutions even with the significant challenges of slow simulation and of complexity in the specification of muscles and/or activation. Much of the early work in this area leaned heavily on characters with simple complexity to address speed [Coros et al. 2012; Kim and Pollard 2011; Tan et al. 2012] while each utilize different mechanics for activation. Namely, Kim and Pollard [2011] embed a skeleton into deformable body to drive animation, while Coros et al. [2012] build controllers from the soft-body posed into target states. Our muscle system more closely matches that of [Tan et al. 2012], as we model muscles as spring-like curves that add forces along their attachments in their current direction. Barbić et al. [2009] employs a reduced order model to speed up their deformation simulation, along with target shapes created manually. Their pioneering work animates soft-body characters through the reduced simulation with the controller running in the low dimensional subspace of the reduced model [Barbić et al. 2009; Barbić and Popović 2008].

While a tremendous amount of work has been introduced in the last decade that employs deep reinforcement learning (DRL) in the area of articulated control [Mourot et al. 2022], we have seen limited work that employs DRL for soft-body control. One exception to this is SoftCon [Min et al. 2019], a deformable simulation extension of [Tan et al. 2011] for animating underwater creatures with several advances. Min et al. [2019] combines a novel muscle excitation/propagation model with DRL to successfully learn the control policies of soft-bodied animals. Their work employs FEM [Sifakis and Barbić 2012] over triangulation [Hu et al. 2018] derived for relatively low resolution character models. Nonetheless, their characters are among the most expressive of those generated showcasing a wide range of behavior results. There is also increasing interest in the development of DRL gym frameworks for soft body problems [Schegg et al. 2022].

It is also worth noting that parallel work has been ongoing in soft robotics [Cheney et al. 2014; Coevoet et al. 2017; Della Santina et al. 2023], with several cross-over works, among these are [Bern et al. 2019; Hu et al. 2019b; Liang et al. 2023].

2.2 Trajectory Optimization

Given keyframe information from the user, the production of control using out differential solver bares some resemblance to work in trajectory optimization. Rather than cast the simulation control as a initial value problem with iterative search, trajectory optimization seeks to solve an entire trajectory simultaneously. Early work in this area, so-called spacetime solvers cast very simple dynamics as constraints that were upheld as acceleration values were computed [Cohen 1992; Ngo and Marks 1993; Witkin and Kass 1988].

Since the introduction of spacetime optimization, several researchers have proposed mechanisms for incorporating trajectory optimization to solve varying character animation control problems [Al Borno et al. 2012; Bern et al. 2019; Liu et al. 2005; Mordatch and Todorov 2014; Safanova et al. 2004; Zordan et al. 2014], among others. A key difference with our problem domain is the incorporation of soft-body dynamics. Deformable simulation introduces significantly

more complex contact conditions, which foils many of the underlying assumptions of the previous work. As such, to solve our desired control problem, we introduce a novel differentiation tool that allows efficient second-order evaluation so that we can use high-order optimization to overcome the inherent nonlinearities.

2.3 Differentiation & differentiable simulation

Evaluating the derivative for differentiation of the loss function is an indispensable step for inverse problems. A commonly used differentiation technique is automatic differentiation or AD [Bartholomew-Biggs et al. 2000; Corliss et al. 2013; Griewank and Walther 2008], which decomposes complicated functions with the chain rule. AD has been extensively used in graphics [Grinspun et al. 2003; Guenter 2007]. Back propagation [Hecht-Nielsen 1992] widely used by the machine learning community training is a special implementation of the reverse AD. AD also forms the foundation of many differentiable simulation frameworks [Du et al. 2021; Hu et al. 2019a,b]. While one may perform AD multiple times to obtain a high-order derivative, it has been argued that recursively applying AD leads to inefficient and numerically unstable code [Betancourt 2018; Margossian 2019].

In contrast to AD, numerical differentiation is also popular. The standard approach is the finite difference method, which however suffers from the *subtractive cancellation* issue: decreasing the magnitude of the perturbation will diverge the calculation [Brezillon et al. 1981]. CSFD is a finite difference scheme based on the complex version of Taylor series expansion [Lyness 1967]. It has been used for nonlinear FEM [Kim et al. 2011; Luo et al. 2019] and sensitivity analysis [Anderson et al. 2001; Montoya et al. 2015]. While it is possible to directly use CSFD to compute high-order derivatives [Shen et al. 2021] by generalizing regular CSFD to multi-complex numbers. It requires excessive forward function evaluations and is prohibitive if the actual derivative is needed (e.g., in Newton's method).

We posit that achieving high-order differentiation for general-purpose and complicated computations should be enabled in a hybrid way, by leveraging the best of both numerical and analytic differentiation modalities. This allows an efficient gradient calculation without significantly increasing the order of the differentiation in each modality. To this end, we propose a novel CSFD-AD differentiation scheme. By treating AD as a black-box computation and promoting it with CSFD, we can conveniently obtain the gradient of AD's output or, subsequently, the Hessian of the target loss.

Our method is also relevant to differentiable IPC simulation [Huang et al. 2022], which uses the adjoint method [Givoli 2021] to calculate the loss gradient. Unfortunately, high-order adjoint method remains a research problem, and it becomes less help for elastic locomotion, for which second-order descent information is essential. Our method, on the other hand, can effectively obtain the Hessian for the use of higher-order optimizations to optimize the target loss, which is very useful for dealing with complex collision situations.

3 OVERVIEW

Fig. 2 outlines major steps of our pipeline and their corresponding discussions in the paper. Elastic locomotion embodies a standard inverse problem. Given a soft object embedded in a set of both contractile and extensible muscle fibers, elastic locomotion estimates

necessary activation forces along the muscle fibers that enable natural and coordinated movement of the object under user-prescribed high-level motion descriptors e.g., the body trajectory. While muscle activations are the driving force, it is frictional contacts between the environment that play a key role in the body's locomotion. Elastic locomotion decomposes the high-dimension space-time optimization problem into sequential nonlinear programming frame by frame. At each frame, we use a mixed differentiation modality, which efficiently returns the first- and second-order gradient information (w.r.t. the target loss function), and it is agnostic to the specific simulation algorithm adopted nor the total number of interactions used. The second-order descent direction is indispensable for such a strongly nonlinear inverse problem. In the following sections, we elaborate on each of the major steps in detail.

4 PROBLEM FORMULATION

We discretize a 3D soft object with a tetrahedral mesh of N nodes and embed muscle fibers in its body as the primary motion driver. The equation of motion of this deformable object is modeled using nonlinear FEM and implicit Euler, in the form of force equilibrium as:

$$\begin{aligned} \mathbf{x}_{t+1} &= \mathbf{x}_t + \Delta t \mathbf{v}_{t+1}, \\ \mathbf{v}_{t+1} &= \mathbf{v}_t + \Delta t \mathbf{M}^{-1} (\mathbf{f}_{int} + \mathbf{f}_{ext} + \mathbf{f}_d + \mathbf{f}_c + \mathbf{f}_m), \end{aligned} \quad (1)$$

where $\mathbf{M} \in \mathbb{R}^{3N \times 3N}$ is the mass matrix, \mathbf{f}_{int} , \mathbf{f}_{ext} , \mathbf{f}_d , \mathbf{f}_c , \mathbf{f}_m represent elastic (i.e., internal), external, damping, contact and muscle forces, respectively, Δt is the time step size, and \mathbf{x}_t and velocities \mathbf{v}_t at time step t .

The elastic force is the resultant force produced by the elastic properties of a material that resists deformation. It is calculated as the negative gradient of the elastic potential energy. In our implementation, we use the stable Neo-Hookean energy [Smith et al. 2018]:

$$\Psi = \frac{\mu}{2} (I_C - 3) - \mu(J - 1) + \frac{\lambda}{2} (J - 1)^2, \quad (2)$$

where $I_C = \text{tr}(\mathbf{F}^\top \mathbf{F})$ and $J = \det(\mathbf{F})$ are computed based on the deformation gradient \mathbf{F} . Terms μ and λ are Lamé constants. Nevertheless, our pipeline is compatible with any hyperelastic material models. The external force, attributable to gravity, is constant. We use the Rayleigh damping to calculate the damping force:

$$\mathbf{f}_d = (\alpha \mathbf{M} + \beta \mathbf{K}_0) \mathbf{v}_{t+1}, \quad (3)$$

where \mathbf{K}_0 is the rest-shape stiffness matrix. The contact force is evaluated following the IPC formulation. IPC activates a barrier potential energy B if a surface triangle is sufficiently close to a collider:

$$B(d, \hat{d}) = \begin{cases} -\kappa(d - \hat{d})^2 \ln\left(\frac{d}{\hat{d}}\right), & 0 < d < \hat{d}, \\ 0, & d \geq \hat{d}. \end{cases} \quad (4)$$

Here, d stands for the distance between the triangle and the collider; \hat{d} is the constraint tolerance ($\hat{d} = 1E - 3$ in our implementation); and κ is a hyper-parameter controlling the initial stiffness of the barrier. The negative gradient of the barrier gives the collision force at (nearly) contacting triangles. The friction force is evaluated in a

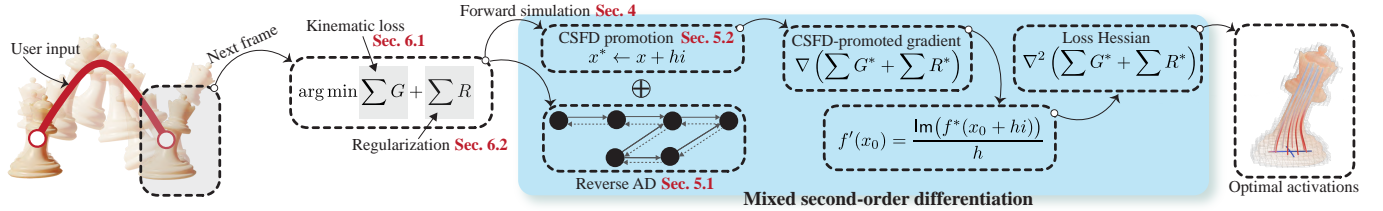


Fig. 2. An overview of our computational pipeline. Elastic locomotion solves an inverse simulation problem. The user specifies high-level kinematic targets the body expects to achieve, which is formulated as a scalar-value loss function combining the target function and regularization terms. We use classic line-search Newton to solve this problem. The Hessian of the loss function is obtained by our mixed second-order differentiation scheme, which combines CSFD and AD to efficiently calculate contact-in-the-loop loss Hessian.

lagged way based on the information of the collision force in the previous iteration.

Similar to [Tan et al. 2012], we model muscle fibers as polygonal curves with M segments. Each muscle segment is modeled as an individual spring that can contract or extend along its current direction, but it does not bend. A segment exerts an activation $a \in \mathbb{R}$ along its direction, either contraction or extension. An activation affects multiple nearby elements. For the i -th element and j -th muscle segment, the influencing weight w_{ij} is based on their geodesic distance g_{ij} on the mesh as a Gaussian kernel:

$$w_{ij} = \exp\left(-\frac{g_{ij}^2}{c^2}\right), \quad (5)$$

where c is the variance of the Gaussian function. w_{ij} only depends on the rest shape of the body and muscle, and it can be pre-computed. The accumulated muscle stress in the deformed coordinates of the element is:

$$\sigma_i = \sum_j w_{ij} R E_j R^\top, \quad (6)$$

where

$$E_j = U \begin{bmatrix} f_j & 0 & 0 \\ 0 & 0 & 0 \\ 0 & 0 & 0 \end{bmatrix} U^\top = \mathbf{d}_j \otimes \mathbf{d}_j a_j. \quad (7)$$

Here, R transforms the stress E_j from the reference coordinates to the deformed coordinates, and U rotates vector $[1, 0, 0]^\top$ in the reference coordinates to align with \mathbf{d}_j , the direction of muscle segments in the reference coordinates. We project the σ_i to the area-weight face normal of the element in the deformed coordinates. This surface force is evenly split to vertices to derive f_m at every node. We use a pose-dependent activation matrix $A \in \mathbb{R}^{3N \times M}$ to encode the muscle force computation, such that:

$$f_m = A(\mathbf{x})a, \quad (8)$$

where $a \in \mathbb{R}^M$ is the vector of activations of all the muscle segments.

Users can design the muscle arrangement in the deformable body to support different control tasks. Several muscle arrangements are shown in Fig. 3. For example, implanting several longitudinal muscle fibers spanning the height allows the body to be shortened through muscle contraction. Body bending can be manipulated via asymmetrical contraction, and body extension/stretching follows relaxing post-contraction. Circular muscles encircle the body, and radial muscles span a cross-section of the body. When these muscles contract, the body thins and gets lengthened due to the volume preserving of the material. Oblique muscles or helical muscles wrap around the body in a helical shape to support twisting. How to deploy such actuators for motion control itself is an interesting research problem [Thelen et al. 2003; Tzoumas et al. 2015]. This however, is not the focus of this paper, and our system assumes a prescribed muscle placement.

4.1 Loss function

We express the objective function in the optimization as:

$$\arg \min_a L(\mathbf{x}, a) = \sum_i w_i G_i(\mathbf{x}_{t+1}, a) + \sum_j \lambda_j R_j(\mathbf{x}_{t+1}, a), \quad (9)$$

where each G_i is a user-defined objective to depict the kinematic state of soft-body motion, such as jumping, twisting, and rolling. Regularization penalty terms R_j are also included (Sec. 6.2). Our method solves for the appropriate muscle contraction and relaxation a to apply the muscle force f_m , ensuring that the position \mathbf{x}_{t+1} of the object at the next time step conforms to the user's description.

This is a challenging optimization problem because \mathbf{x}_{t+1} depends on a implicitly via the equation of motion Eq. (1), which needs to take into account dynamic contacts and friction. While the use of the barrier energy from Eq. 4 obviates the need for complementarity programming, it increases the nonlinearity of the problem. Existing differentiable simulation methods [Du et al. 2021; Huang et al. 2022] are mostly first-order based on the gradient information of the loss function and fail to converge in our problem.

Instead of relying on gradient exclusively, we leverage Newton's method to tackle the nonlinearity induced by contact barriers. Newton's method exhibits superior second-order performance in proximity of a local minimum. Before Newton iterations, we apply several iterations of gradient descent. Gradient descent is less sensitive to

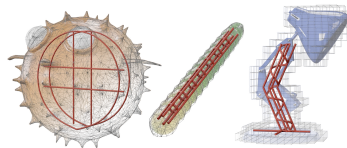


Fig. 3. Muscle arrangement. We highlight the arrangement of muscles in some examples reported in the paper. We assume the muscle setup is provided.

initial selection and offers a reasonable starting point for the follow-up Newton. Naturally, the muscle contraction of the last frame \mathbf{a}_t serves as an initial guess in our process.

5 MIXED DIFFERENTIATION

The method used to solve Eq. (9) is far from novel – it embodies a standard nonlinear procedure with line search. Yet, the challenge is not the optimization itself but the evaluation of the loss Hessian.

5.1 Reverse AD

The loss function $L : \mathbb{R}^M \rightarrow \mathbb{R}$ maps an input activation vector to a scalar-value loss. A common practice is to use reverse AD to calculate its gradient, i.e., by back-propagating the differential from the output to the input, as used in most deep learning frameworks [Hecht-Nielsen 1992]¹.

In reverse AD, the computational process is performed in two phases: a forward pass and a reverse pass. The forward pass computes and stores function values and intermediate results. In the reverse pass, it passes derivatives backward from the output to the inputs, complementing each intermediate variable v_i with an adjoint $\bar{v}_i = \frac{\partial y_i}{\partial v_i}$ representing the sensitivity of output y_i w.r.t. changes in v_i . Take an intermediate step of $v_t = f_k(v_r, v_s)$ for example. Assuming v_a and v_b are not used in other intermediate computations, reverse AD applies the chain rule and gives \bar{v}_a and \bar{v}_b by:

$$\bar{v}_r = \frac{\partial f_k}{\partial v_r} \bar{v}_t, \quad \bar{v}_s = \frac{\partial f_k}{\partial v_s} \bar{v}_t. \quad (10)$$

It is possible to solely use reverse AD to compute the Hessian of a function. Doing so involves two passes of reverse AD. The computational graph, as well as all the intermediate values generated during the first AD invocation, must be saved. The second reverse AD is applied at each component of the resulting gradient vector. This results in significant memory usage because each gradient component also generates a more expansive computational graph. In our problem, \mathbf{x}_{t+1} is related to \mathbf{a} via a barrier-in-the-loop FEM procedure, the memory consumption using AD for Hessian evaluation is prohibitive. In addition, repetitively applying AD for calculating high-order differentiation has been known to be numerically unstable [Margossian 2019].

5.2 CSFD

Alternatively, we inject a different differentiation modality i.e., complex-step finite difference or CSFD, into this procedure to calculate the second-order differentiation of the loss function and avoid aforementioned issues due to consecutive AD invocations. Given a real-value function $f : \mathbb{R} \rightarrow \mathbb{R}$, assume that it is differentiable around $x = x_0$. Conventional finite difference scheme applies a small real perturbation h to x_0 and approximates the function gradient as:

$$f'(x_0) = \frac{f(x_0 + h) - f(x_0)}{h} + O(h). \quad (11)$$

When h gets smaller, $f(x_0 + h)$ and $f(x_0)$ become nearly equal to each other. Subtraction between them eliminates leading significant digits, and the result after rounding could largely deviate from the

¹If the function maps a low-dimension input to a high-dimension output, forward AD is more efficient.

actual value. This stability issue is known as the subtraction cancellation. Therefore, finite difference is not suitable for our problem.

CSFD promotes this function to the complex domain as $f^* : \mathbb{C} \rightarrow \mathbb{C}$. Here, we use $(\cdot)^*$ to denote a complex variable. CSFD applies the perturbation along the imaginary direction to estimate the gradient at $x^* = x_0 + 0i$ as:

$$f'(x_0) = \frac{\text{Im}(f^*(x_0 + hi))}{h} + O(h^2) \approx \frac{\text{Im}(f^*(x_0 + hi))}{h}. \quad (12)$$

Eq. (12) does not have a subtractive numerator, meaning it only has round-off error, regardless of the size of the perturbation h . This allows us to set h sufficiently small to accurately estimate the gradient information. For instance, if $h \sim \sqrt{\epsilon}$ i.e., around 1×10^{-16} , CSFD approximation error is at the order of the machine epsilon ϵ . Hence, CSFD can be as accurate as analytic derivative because the analytic derivative also has a round-off error of ϵ .

5.3 Mixed differentiation

CSFD can be generalized with multi-complex numerics to estimate the high-order differentiation [Luo et al. 2019]. However, doing so needs to apply $O(M^2)$ perturbations to the loss function to obtain each element in Hessian. This is prohibitive for a high-dimension inverse problem like ours. Unfortunately, in order to use Newton’s method, the explicit Hessian matrix has to be assembled. To this end, we combine CSFD and AD to avoid excessive perturbations and an over-expansive computational graph. We treat AD as a generic function which maps the input x to its first-order derivative. Applying CSFD of AD naturally gives us the second-order differentiation of the target function, and we name this mixed differentiation scheme CSFD-AD i.e., CSFD-perturbed (inverse) AD procedure. CSFD-AD follows the AD algorithm but promotes each intermediate variable and adjoint to complex variables: $v_i^*, \bar{v}_i^* \in \mathbb{C}$.

Second-order derivative of the k -th component of the input $[\nabla^2 f]_k = \frac{\partial^2 y}{\partial x_k^2}$ can be computed with a single application of mixed differentiation as:

$$[\nabla^2 f]_k = \lim_{h \rightarrow 0} \frac{\nabla f(x + h\mathbf{e}_k) - \nabla f(x)}{h} \approx \frac{\text{Im}(\nabla f(x + hi \cdot \mathbf{e}_k))}{h}. \quad (13)$$

Here, $[\cdot]_k$ gives k -th column of Hessian matrix, and \mathbf{e}_k is the k -th canonical basis. Eq. 13 allows us to construct Hessian only with M perturbations (instead of M^2 perturbations using high-order CSFD), and those M perturbations can be conveniently parallelized.

Fig. 4 shows an illustrative example of CSFD-AD procedure over a simple computational graph of $f = \mathbf{x} \cdot \mathbf{x} = x_1^2 + x_2^2 + x_3^2$, where $x_1 = 1$, $x_2 = 2$, and $x_3 = 3$. The forward pass propagates the perturbed $x_1^* = 1 + hi$ via the intermediate values v_i^* to the final output $y^* = 14 + 2hi$. Note that the high-order term of h in v_1^* is discarded. Following this, the backward pass uses the original AD algorithm but with all adjoints and computations being complex based. The real part of \bar{x}^* carries the value of the first-order derivative same as normal AD, while the second-order derivative equals the imaginary part of \bar{x}^* upon its division by the input disturbance h . We have further optimized such vector and matrix operations. For more details, please refer to Section 5.5 and the right part of this figure.

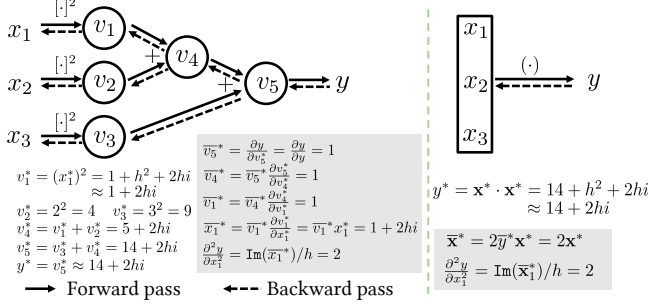


Fig. 4. **CSFD-AD procedure.** We show an illustrative example of using CSFD-AD to compute the self inner product of a 3-vector \mathbf{x} : $f = \mathbf{x} \cdot \mathbf{x}$.

5.4 CSFD overload

Here, we briefly discuss the implementation of CSFD-overload operators and functions in CSFD-AD when used in a computing procedure, as well as their differentiability.

Relational logic operators such as $>$, \geq , $<$, \leq and $==$ are common in computing code but usually not defined for complex numbers. They interact with conditional statements to guide execution flow. We make sure that the results of the original algorithm and its CSFD-overload version match each other e.g., $a^* > b^*$ for $a^*, b^* \in \mathbb{C}$ should always yield the same result as $a > b$. This is done by setting $a^* > b^* \leftarrow \text{Re}(a^*) > \text{Re}(b^*)$. Similarly, single-argument functions such as `max` or `min` only evaluate the real parts of the input.

Conditional statement-driven computations are often discontinuous, leading to multiple branches such as: $f(x) = x$ for $x \geq 0$ and $f(x) = 2x$ for $x < 0$. CSFD applies the perturbation in the imaginary direction, which is orthogonal to the real axis. As a result, it always returns the differentiation of the function at the branch of $f(\text{Re}(x_0^*))$. In this example, if $\text{Re}(x_0^*) \geq 0$, CSFD yields the gradient of $f(x) = x$. On the other hand, if $\text{Re}(x_0^*) < 0$, CSFD yields the gradient of $f(x) = 2x$. There is no special treatment of safeguard needed.

Arithmetic operators include $+$, $-$, \times , $/$ and functions include \sin , \log , \exp , just name a few. Most of these elementary functions are *analytic* on complex domain, i.e., the complex function $f^*(a+bi) = u(a,b) + v(a,b)i$ satisfies the Cauchy-Riemann equations:

$$\frac{\partial u}{\partial a} = \frac{\partial v}{\partial b}, \quad \frac{\partial v}{\partial a} = -\frac{\partial u}{\partial b}. \quad (14)$$

A complex function that is analytic exhibits differentiability on its domain around $x_0^* = a_0 + b_0i$ means that it can be differentiated infinitely many times, and CSFD-AD always yields correct results. For instance, the complex promotion of $\sin(x)$ is $f^*(x^*) = \sin(a+bi) = \sin(a)\cosh(b) + \cos(a)\sinh(b)i$, since $\frac{\partial u}{\partial a} = \cos(a)\cosh(b) = \frac{\partial v}{\partial b}$, and $\frac{\partial v}{\partial a} = \sin(a)\sinh(b) = -\frac{\partial u}{\partial b}$. Similarly, we have $\cos(a+bi) = \cos(a)\cosh(b) - \sin(a)\sinh(b)i$.

During the backward pass of CSFD-AD, the complex-promoted adjoint is $\bar{x}^* = \cos(x^*)\sin(x^*)$, which can be expand as:

$$\begin{aligned} \bar{x}^* &= \cos(a)\cosh(b)\text{Re}(\sin(x^*)) + \sin(a)\sinh(b)\text{Im}(\sin(x^*)) \\ &+ \left(\cos(a)\cosh(b)\text{Im}(\sin(x^*)) - \sin(a)\sinh(b)\text{Re}(\sin(x^*)) \right) i. \end{aligned} \quad (15)$$

In general, if a real-value function f is differentiable around x_0 , and its complex version is irrelevant to its complex conjugate $x_0^{*C} = a_0 - b_0i$, it satisfies the Cauchy-Riemann equations and therefore complex-differentiable.

The absolute value function `abs` however, is an expectation. Standard complex `abs` function defined as $f^*(x^*) = |a+bi| = \sqrt{x^* \cdot x^{*C}} = \sqrt{a^2 + b^2}$ always returns a positive non-negative number for complex inputs. It corresponds to the magnitude of x^* . While a bit counter-intuitive, this function does not satisfy the Cauchy-Riemann identities, and it is *not* analytic (and cannot be used in CSFD). To this end, we derive an analytic form of the absolute value function:

$$\text{abs}(a+bi) = \begin{cases} -a - bi, & \text{if } a < 0, \\ ax + bi, & \text{if } a \geq 0. \end{cases} \quad (16)$$

When CSFD-AD is applied, the adjoints are:

$$\bar{x}^* = \begin{cases} -\overline{\text{abs}(a+bi)}, & \text{if } a < 0, \\ \overline{\text{abs}(a+bi)}, & \text{if } a \geq 0. \end{cases} \quad (17)$$

The chain rule forms the foundation of AD, which allows local differentials to be assembled to be the global differentiation. CSFD-AD also uses the chain rule in the backward pass. The generalized chain rule for complex valued function $y^* = f^*(x^*)$ and $z^* = g^*(y^*) = g^*(f^*(x^*))$ can be applied as:

$$\frac{\partial z^*}{\partial x^*} = \frac{\partial g^*(y^*)}{\partial x^*} = \frac{\partial g^*}{\partial y^*} \frac{\partial y^*}{\partial x^*} + \frac{\partial g^*}{\partial y^{*C}} \frac{\partial y^{*C}}{\partial x^*}, \quad (18)$$

If a function is analytic, the second term reduces to zero, and the equation restores to the normal chain rule for real numbers. Under this circumstance, the back-propagation process of CSFD-AD is consistent with AD, except that the computation rule needs to follow the complex number operation.

5.5 Matrix data structures and arithmetic

We use the Eigen C++ Library as our primary complex-value matrix and vector container. Applying AD to some matrix operations could produce a large number of redundant nodes and edges on the computational graph. For example, the squared norm of an N -dimension vector is computed as: $\|\mathbf{x}\|^2 = \mathbf{x} \cdot \mathbf{x} = x_1 \cdot x_1 + x_2 \cdot x_2 + \dots + x_N \cdot x_N$. It takes N multiplications and $N - 1$ additions, and therefore introduces $2N - 1$ nodes for storing and computing intermediate results and adjoints. We eliminate this memory and computing overhead by implementing a specialized function for $y = f(\mathbf{x}) = \|\mathbf{x}\|^2$: $\bar{x} = 2\bar{y}\mathbf{x}$, which only needs N adjoints for \bar{x} .

5.6 Linear algebra decomposition and factorization

We implement CSFD-AD to support most known linear algebra functions including trace, determinant, inverse and singular values. We list a few commonly used ones in Tab. 1. Singular value decom-

Table 1. CSFD-AD for matrix operation. We list CSFD promotions of matrix functions that we have implemented for elastic locomotion.

Function	\bar{X}	Function	\bar{X}^*
$z^* = \ \mathbf{x}^*\ ^2$	$2\bar{z}^* \mathbf{x}^*$	$z^* = \mathbf{x}^{*\top} \mathbf{y}^*$	$\bar{z}^* \mathbf{y}^*$
$Z^* = \mathbf{X}^* \mathbf{B}^*$	$\bar{Z}^* \mathbf{B}^{*\top}$	$Z^* = \mathbf{A}^* \mathbf{X}^*$	$\mathbf{A}^{*\top} \bar{Z}^*$
$z^* = \mathbf{A}^{*-1} \mathbf{x}^*$	$\mathbf{A}^{*-1} \bar{z}^*$	$z^* = \mathbf{X}^{*-1} \mathbf{b}^*$	$-\mathbf{X}^{*-1} \bar{z}^* \mathbf{z}^{*\top}$
$z^* = \text{tr}(\mathbf{X}^{*\top} \mathbf{X}^*)$	$2\bar{z}^* \mathbf{X}^*$	$z^* = \det(\mathbf{X}^*)$	$\bar{z}^* \mathbf{z}^* \mathbf{X}^{*\top}$

position (SVD), $\mathbf{A} = \mathbf{U} \Sigma \mathbf{V}^\top$, is a widely used numerical procedure in FEM simulation e.g., to extract the invariants of the deformation gradient. While SVD of such 3×3 has a closed-form formulation, resulting singular values of a complex matrix are always real (e.g., similar to complex abs). Therefore, SVD operation is not analytic, and CSFD promotion cannot be applied to its closed form. Alternatively, we apply CSFD-AD to the iterative numerical SVD procedure for real matrices and overload each underlying operation with complex arithmetics. In our implementation, we employ implicit-shifted symmetric QR SVD [Gast et al. 2016] for fast and robust decomposition on symmetric 3×3 matrices.

Elastic locomotion needs to solve a sparse system at each Newton iteration in the form of $\mathbf{A}\mathbf{x} = \mathbf{b}$. We use direct solvers like LU, LLT, and LDLT to handle those linearized system solves. Unlike SVD, matrix factorization is analytic, and CSFD promotion can be directly applied. However, doing so expands the computational graph exponentially in the first AD pass. Therefore, we compute the adjoints of the solution of the linear solve: $\mathbf{b} = \mathbf{A}^{-1} \mathbf{x}$. During the forward pass, the factorized matrix of \mathbf{A} is stored; and in the backward pass, the adjoint of the linear solve i.e., $\bar{\mathbf{b}}$ is then obtained by solving $\bar{\mathbf{b}} = \mathbf{A}^{-\top} \bar{\mathbf{x}}$ using the saved factorization of \mathbf{A} . This strategy is similar to the adjoint method [Givoli 2021], which frees us from obtaining the actual adjoints of the matrix inverse. Alternatively, it is also possible to apply CSFD promotion to a numerical iterative linear solver as in many existing differentiable simulation frameworks [Du et al. 2021; Hu et al. 2019a]. Doing so requires the total number of iterations to be pre-known. Therefore, existing methods often use a prescribed iteration count. This is a risky measure: too few iterations will cause the solver to diverge, while an over-conservative setting consumes too much memory since the computational graph expands proportional to the number of iterations. Elastic locomotion involves nonlinear contact barriers, and the variation of iteration counts is substantial depending on the actual configuration of contacts and frictions. Therefore, assuming a fixed iteration number is not an option for us.

6 LOCOMOTION CONTROL

The mixed differentiation modality with CSFD-AD offers a generic way to evaluate high-order differentiation of a complex computation procedure. Therefore, our system is compatible with a wide range of intuitive controllers to allow the user to manipulate, author, and design the locomotion of soft objects via high-level kinematic objectives. We also design an intuitive user interface to facilitate such edits. In this section, we describe some loss functions used in our examples.

6.1 Target functions

Linear motion controllers. We achieve the desired locomotion mainly by controlling the target trajectory of some key points on the object. For the position of a target point \mathbf{x}^* , the objective function that constrains the position can be written as:

$$G_{\text{position}} = \|f(\mathbf{x}) - \mathbf{x}^*\|^2, \quad (19)$$

where f could refer to the calculation of the COM (center of mass) $\mathbf{c} = f_{\text{COM}}(\mathbf{x})$ of the body, of local COM coordinates (foot, head, base, etc.), or of the relative position between points. We also use similar objective functions to track the velocity:

$$G_{\text{vel.}} = \left\| f\left(\frac{\mathbf{x} - \mathbf{x}_t}{\Delta t}\right) - \mathbf{v}^* \right\|^2, \quad (20)$$

and acceleration:

$$G_{\text{acc.}} = \left\| f\left(\frac{\mathbf{x} - 2\mathbf{x}_t + \mathbf{x}_{t-1}}{\Delta t^2}\right) - \mathbf{a}^* \right\|^2. \quad (21)$$

For instance, we could specify the starting speed of the character to achieve jumps of different heights in addition to its COM target, and we control the relative speed of the character’s head and base to achieve the aerial posture of the forward jump. We can achieve object lift-off by setting the COM acceleration \mathbf{a}^* equal to the gravitational acceleration. The control over the COM acceleration is also equivalent to the control of the derivative of the linear momentum $\dot{\mathbf{L}} = m\dot{\mathbf{c}}$, which takes part in balance control [Tan et al. 2012].

Angular motion controllers. We control the rotation of the body around an axis by manipulating the changes in the body’s angular momentum:

$$G_{\text{angular}} = \|\dot{\mathbf{L}}_{\text{angular}}(\mathbf{x}) - \dot{\mathbf{L}}^*\|^2, \quad (22)$$

where $\mathbf{L}_{\text{angular}} = \sum_i m\mathbf{r}_i \times \dot{\mathbf{v}}_i$ is the total angular momentum of the collection of points. This objective is typically used to control the rotation and twisting of an object on the ground, such as allowing the character to gain sufficient angular velocity before it flips and jumps in the air. If a body that wants to perform a flip movement in the air, we control the body’s moment of inertia (MOI) $\mathbf{I} = \sum_i m_i \mathbf{r}_i^2$ around the axis to make the character contract and rotate faster. This is also a common technique used by diving athletes.

$$G_{\text{MOI}} = \|\dot{\mathbf{I}}(\mathbf{x}) - \dot{\mathbf{I}}^*\|^2. \quad (23)$$

Additional control variants. Thanks to the CSFD-AD differentiation algorithm, our framework allows users to use sophisticated target functions without manually deriving their closed-form derivatives. For instance, controlling the changes in elastic energy of an object:

$$G_{\text{elastic}} = \left\| \int \dot{\Psi} dV - \dot{E}^* \right\|^2, \quad (24)$$

where the integral applies over a specific portion of the body. This objective function plays an essential role in the jumping experiment shown in Fig. 11. By specifying the change in the potential energy of the trampoline, we can control the future kinetic energy of the lamp, allowing the lamp to reach different heights.

We also control the size of the projection base area, allowing the object to expand its base to maintain balance during the landing

Table 2. Time statistics. This table reports simulation setups and time performance of examples shown in the paper. # Ele. is the total numbers of elements on the body. $|\alpha|$ is the dimension of control variables i.e., muscle activations. N_c reports the maximum number of contacts processed per time step. Sim, Grad, Hess and Solve give the average timing of forward simulation, gradient computing, Hessian computing and total solving time in seconds per time step.

Soft body	# Ele.	$ \alpha $	N_c	Sim	Grad	Hess	Solve
Caterpillar Figs. 7,9	2.6K	62	140	0.8	0.5	5.2	15.4
Starfish Fig. 8	2.8K	66	192	0.9	0.5	6.2	20.3
Chess Fig. 10	8.4K	72	224	1.4	1.0	12.8	36.6
Lamp Figs. 1, 11	5.2K	68	166	1.1	0.9	8.8	19.5
Stool Fig. 12	6.8K	40	246	1.0	0.6	4.8	21.6
“T” Fig. 13	1.2K	51	25	0.2	0.2	3.4	5.5
Puffer fish Fig. 14	27.6K	32	171	4.7	2.8	27.1	68.6

process of continuous jumps:

$$G_{proj} = \|\dot{A}_{proj}(\mathbf{x}) - \dot{A}^*\|^2, \quad (25)$$

where A_{proj} returns the projection area of the body on some contacting or supporting plane. The strategy of designing and choosing the most effective controller is the core problem of animation control and a wide range of specific motion planning problems. This is not the focus of this work. Nevertheless, we do believe CSFD-AD delivers a useful computational tool, and it could enable more creative and versatile controllers.

6.2 Regularization terms

We design regularization terms to enhance the stability of the optimization process, i.e., the Hessian of the objective function Eq. (9) is positive definite. This is similar to the LM method [Moré 2006]. Specifically, we regulate the total muscle energy to avoid conflicting or excessive muscle actions that would cause energy waste and trigger improbable distortion:

$$R_{energy} = \frac{1}{2}k\|\alpha\|^2, \quad (26)$$

where $k > 0$ controls the strength of the regularization.

In addition, we impose penalties on muscle segments whose rate of change $|\dot{\alpha}_i|$, exceeds a pre-defined threshold $\dot{\alpha}_{max}$:

$$R_{change} = \sum_i (|\dot{\alpha}_i| - \dot{\alpha}_{max})^2, \quad \forall |\dot{\alpha}_i| > \dot{\alpha}_{max}. \quad (27)$$

7 RESULT

We implemented our framework on a desktop computer with an Intel i9-13900KF CPU with 128GB of memory. We developed our CSFD-AD framework based on Stan Math library [Carpenter et al. 2015] (for reverse AD) and Eigen Library [Guennebaud et al. 2010] (for complex linear algebra and matrix interface). We implemented the complex promotion of all analytic functions by ourselves. We enabled Intel TBB [Pheatt 2008] for parallel processing of Hessian calculations in multiple threads. The detailed statistics of experiments are reported in Table 2. The time step size is set as $\Delta t = 1/40$ sec in all the experiments. Please refer to the supplementary video for animated results.

7.1 Comparison with gradient descent and L-BFGS

The first experiment we would like to report is to highlight the need of a second-order optimizer of inverse control problems. To this end, we compare the results using gradient-based methods and Newton’s method through a basketball shooting experiment, as shown in Fig. 6. In this experiment, an I-shaped soft body pushes a ball to pass a basket ring. Observing the projection plane, the initial position of the ball is $(0, 1.5)$, and the basket of radius 0.5 is at $(1.5, 2)$. The body first contracts, bends forward and then releases. Before releasing, it has to ensure that the relationship between the speed and position of the ball’s COM is satisfied in order to generate the right contact force to push the ball to fall into the basket.

In the figure, the blue curve GD (a) visualizes the trajectory if we only use gradient information (with 1,000 iterations) for solving Eq. (9) e.g., as in [Hu et al. 2019a,b]. The ball fails to follow the prescribed path and does not even reach the basket due to lesser convergence. The green curve Newton (a) is the result of our method with second-order optimization – the ball passes through the basket ring accurately. Even if we switch to gradient descent only at the last time step before the body releases the ball, the resulting trajectory is still inaccurate (the orange curve GD (b)), where the ball bounces back from the rim. The red curve Newton (b) shows the result of second-order optimization for another target trajectory, where the soft-body player scores again.

We further compare our method with gradient descent and L-BFGS [Du et al. 2021; Huang et al. 2022] in several representative scenes of different combinations of loss functions. The results are shown in Fig. 5. In the figure, x -axis represents the number of iterations after the same warm start, and y -axis is the value of the loss function (the low the better). Our method demonstrates strong second-order convergence in all examples. The convergence gap is widened if the specific frame contains a large number of frictional contacts. On the other hand, there is no contact, L-BFGS also gives a good convergence (e.g., see the fourth plot in Fig. 5). Meanwhile, gradient descent does not offer the desired convergence in all cases.

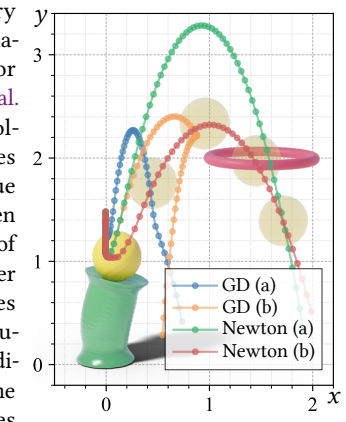


Fig. 6. Comparison with gradient descent. An I-shaped soft-body player tries to “shoot” a ball into a basket under user-specific trajectory. Gradient descent fails to converge the loss sufficiently, while the soft-body player always secures the score with Newton’s method (ours).

7.2 Comparison with LCP-based contact resolution

The contact and friction between the soft body and the environment are often the most challenging aspects of locomotion control. Complementarity programming is an accurate math model of the contact problem but its convergence is not guaranteed. This drawback becomes more severe for elastic locomotion because a soft body

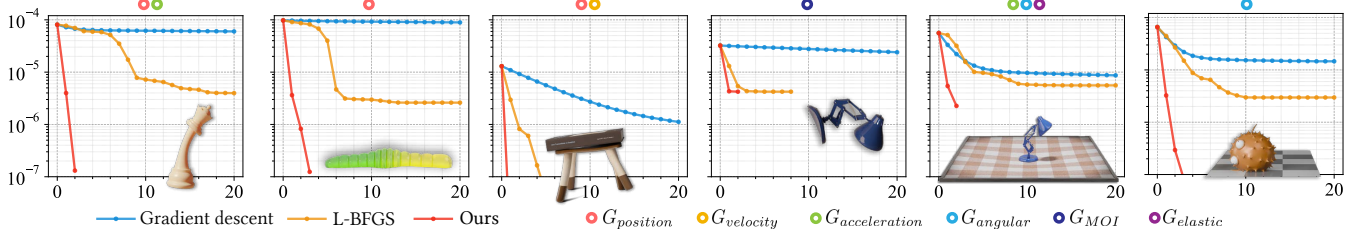


Fig. 5. **Convergence curves under different combinations of losses.** We compare the convergence performance using gradient descent [Hu et al. 2019a], quasi-Newton (L-BFGS) [Du et al. 2021; Huang et al. 2022], and full Newton (our method) at some representative frames of different elastic locomotions and combinations of loss functions. Newton’s method consistently outperforms other optimization algorithms after a proper warm start. If the body does not undertake extensive collisions (e.g., the third and fourth plots), L-BFGS also yields good convergence.

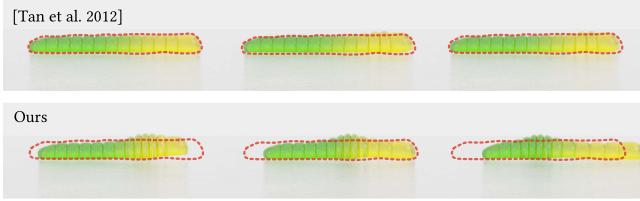


Fig. 7. **Gummy caterpillar (comparison with [Tan et al. 2012])** A soft gummy caterpillar moves on the ground. Such motion is enabled by a combination of stretching and contracting of the body under persistent body-ground contacts. Such sophisticated locomotion involves a large number of contact points and frequent switches between sticking and sliding friction. LCP-based solvers [Tan et al. 2012] become extremely slow in finding a usable solution, and the caterpillar barely moves. Our method, on the other hand, leveraging IPC and line-search Newton, helps the caterpillar move forward as expected.

often uses wide contact regions to adjust its pose and motion. For instance, Tan et al. [2012] solve the body collision using the QPCC solver. In [Tan et al. 2012], each contacting point has 10 contact states, and the minimizer is found in the solution space of 10^N . In the worst case, they need to perform an exhaustive search to obtain a global minimizer. This is prohibitive for soft bodies of moderately high resolution, as we can easily have dozens of contact points. An early termination of the combinatorial search could leave the body in an ill-defined configuration. To mitigate this difficulty, Tan et al. [2012] only supports the solution of four contact patches. This, in turn, reduces the accuracy of the contact model.

Our framework follows the interior-point method to use impulse-like (but smooth) contact barriers to model contact and friction. As a result, our method supports complex contact modeling. A representative example is shown in Fig. 7. In this example, we control a gummy caterpillar to crawl forward on the ground. There are 140 contact points in total, and the muscles embedded trigger alternations between contractions and expansions at body parts contacting the ground. The contact states of those points vary at each frame. In this case, the QPCC solver and search strategy proposed in [Tan et al. 2012] cannot obtain a usable approximate within a reasonable amount of time. Our method, on the other hand, is less sensitive to the number of contact points. The strong convergence of Newton’s method robustly helps find a good solution at each frame.

7.3 More results

We have tested elastic locomotion under an array of scenarios. Thanks to the accurate and efficient evaluation of the Hessian, our method allows the user to animate elastic bodies in various forms and produce interesting animations.

Crawling. In nature, soft-bodied creatures such as worms, slugs, caterpillars, and certain types of mollusks and aquatic animals exhibit unique methods for crawling. Fig. 8 shows a crawling animation of a starfish.

One common crawling method seen in soft creatures is called peristalsis or wave-like motion. For instance, earthworms move through soil using this principle. Their bodies, made of a long series of muscle segments, alternately contract and expand, generating a wave from the anterior to the posterior of the body. As each segment of the worm contacts the soil, it expands, generating friction against the ground. This wave-like motion propels the animal forward through the environment.

We demonstrate such locomotion using a model of a gummy caterpillar in Fig. 9. The target involves dividing the gummy worm model into five separate segments from head to tail to detail the varying states of contraction and relaxation. It implements a sinusoidal function to generate the trajectory of these five parts due to their inherent periodicity, which mirrors the cyclical pattern of muscle movement. Inside the body of the model, we have placed four longitudinal muscles and seven circular muscles. The optimized result is realistic and interesting. Beginning with the longitudinal muscles, their contractions shorten the body, causing it to broaden and rise slightly. Once these muscles relax following the contraction, the body then elongates and flattens out, reaching further forward. On the other hand, the circular muscles run around the body vertically. When these muscles contract, they cause the body to elongate and thin out. Afterward, when the circular muscles relax, the body returns to its original, more rounded shape.

Jumping. Jumping soft-bodied characters are more commonly seen in cartoons and animations. We have replicated the jumping action of Pixar’s Luxo Jr., but in a soft-bodied and physics-based manner. In addition, we have also designed an animation of a game of chess, where the soft-bodied chess pieces move across the board by continuously jumping, as shown in Fig. 10.



Fig. 8. **Crawling starfish.** A starfish moves its legs, adjusts its posture, and displaces to the right. This locomotion involves 192 contact points. LCP-based methods are unable to find a good solution.



Fig. 9. **Crawling caterpillar.** A gummy caterpillar (e.g., the same model in Fig. 7) crawls following the user-provided trajectory. This motion is more challenging than the one shown in Fig. 7 since the friction is asymmetrical along the body in order to generate the curved trajectory.



Fig. 10. **Jumping chess.** The queen in chess performs consecutive leaps forward to declare a check. This example also shows that we may avoid a full space-time optimization if the inverse problem at each frame can be accurately solved.



Fig. 11. **Trampoline acrobatics.** Our method is able to handle high-dimension and complex contact between the body and deformable objects. In this example, a lamp jumps on a trampoline doing a backflip. We adjust the target elasticity potential Eq. (24) to control the level height of each jump.

We divide the jumping process into takeoff phase, mid-air phase and landing phase and apply different controllers accordingly. During the takeoff phase, we first control the position and velocity of COM to compress the body then quickly reverse into a rapid relaxation, releasing the built-up potential energy and increasing contact against the ground to overcome gravity force and follow the target trajectory. The jumping direction and velocity are more accurately handled by our second-order optimization process since the soft body doesn't have control over its trajectory during the mid-air phase. During the mid-air phase, we control the relative velocity of the center of base (COB) and COM to make a fore jump or the angular velocity to make a flip. After that, the soft body expands its base and decreases the velocity of COB to make a softer landing.

The body can then immediately start preparing for another jump, or continue with other types of locomotion.

In our teaser figure (Fig. 1), the lamp jumps onto the stool and then onto the glass coffee table. The friction coefficient of the glass is smaller (0.1), so the lamp controls the position of COM and the contact surface to slide on the table without losing balance. Then, it performs a front flip. During the flip, the lamp reduces its moment of inertia to obtain a greater angular speed. After landing, the lamp rotates and jumps towards the camera.

We also demonstrate a motion involving the collision between the soft character and the deformable environment. In Fig. 11, the lamp bounces on a deformable trampoline multiple times. When it lands on the trampoline, the objective function is designed as the total

elastic potential energy of the trampoline. In the first three jumps, we increment the elastic potential energy objectives so that the lamp jumps higher each time. During the mid-air phase, We switch between different objective functions to make the lamp maintain its shape, backflip and rotate.

Walking. Fig. 12 shows a walking example. We create the walking pattern by lifting and moving one leg from one side while simultaneously doing the same with the opposite diagonal leg. The stool carries a heavy book, moves forward carefully and lets the book slide down slowly. The target functions involve trajectories of four feet to move forward, as well as the position and direction of the carried book to control it to being held when moving or slid down to other books.

Rolling & rotating. We first show a classic locomotion result of a T-shaped character. In this example, the ground contact is relatively simple. We find that both our method and [Tan et al. 2012] can produce similar results following the user’s input. The T-body jumps, lands, and rotates just like a live creature.

A more interesting and complicated scene is shown in Fig. 14. A puffer fish rolls left and right, jumps onto the platform, and reaches the star at the target location. We have added four ring muscles inside the puffer fish to allow for local deformations and used G_{angular} to control its angular momentum changes. We observed that the puffer fish can move its center of mass in front of the center of pressure to continually roll forward. Thanks to the robustness of IPC and Newton, the spikes of the puffer fish can be reasonably deformed during movement without incurring inversion or collapse. Unfortunately, [Tan et al. 2012] is unable to generate this motion with QPCC.

8 CONCLUSION & LIMITATION

This paper shows a novel differentiation strategy combining numerical differentiation (CSFD) and analytic differentiation (reverse AD) to enable efficient calculation of Hessian of a barrier-in-the-loop inverse simulation procedure. We apply this method to calculate the optimal muscle activations, which drive the locomotion of soft bodies under frictional contacts. Our approach is general, and we anticipate it will benefit other application areas where stability is at odds with constrained optimization. Our choice to focus on soft-body control aims to address a lack of solutions for employing such characters in animation, but the approach we introduce has no direct ties to the specifics of deformation simulation and control, such as robotics and fabrication.

Our method also has limitations. While CSFD-AD is more efficient in calculating the Hessian automatically than existing differentiation schemes, assembly of a large-scale Hessian is expensive and at least $O(N^2)$. It is possible to integrate CSFD-AD with other optimization algorithms that do not need the Hessian explicitly, such as L-BFGS. We choose reverse AD for gradient calculation because our loss function is a many-to-one map. Developing CSFD-AD with forward AD is preferred for computations generating high-dimension output from mapping low-dimension input.

REFERENCES

Mazen Al Borno, Martin De Lasa, and Aaron Hertzmann. 2012. Trajectory optimization for full-body movements with complex contacts. *IEEE transactions on visualization and computer graphics* 19, 8 (2012), 1405–1414.

W Kyle Anderson, James C Newman, David L Whitfield, and Eric J Nielsen. 2001. Sensitivity analysis for Navier-Stokes equations on unstructured meshes using complex variables. *AIAA journal* 39, 1 (2001), 56–63.

Jernej Barbic, Marco da Silva, and Jovan Popović. 2009. Deformable object animation using reduced optimal control. In *ACM SIGGRAPH 2009 papers*. 1–9.

Jernej Barbic and Jovan Popović. 2008. Real-time control of physically based simulations using gentle forces. *ACM transactions on graphics (TOG)* 27, 5 (2008), 1–10.

Michael Bartholomew-Biggs, Steven Brown, Bruce Christianson, and Laurence Dixon. 2000. Automatic differentiation of algorithms. *J. Comput. Appl. Math.* 124, 1-2 (2000), 171–190.

James M Bern, Pol Banzet, Roi Poranne, and Stelian Coros. 2019. Trajectory Optimization for Cable-Driven Soft Robot Locomotion. In *Robotics: Science and Systems*, Vol. 1.

Michael Betancourt. 2018. A geometric theory of higher-order automatic differentiation. *arXiv preprint arXiv:1812.11592* (2018).

Patrick Brezillon, Jean-François Staub, Anne-Marie Perault-Staub, and Gérard Milhaud. 1981. Numerical estimation of the first order derivative: approximate evaluation of an optimal step. *Computers & Mathematics with Applications* 7, 4 (1981), 333–347.

Bob Carpenter, Matthew D. Hoffman, Marcus Brubaker, Daniel Lee, Peter Li, and Michael Betancourt. 2015. The Stan Math Library: Reverse-Mode Automatic Differentiation in C++. <https://doi.org/10.48550/arXiv.1509.07164> arXiv:1509.07164 [cs]

Nick Cheney, Robert MacCurdy, Jeff Clune, and Hod Lipson. 2014. Unshackling evolution: evolving soft robots with multiple materials and a powerful generative encoding. *SIGEVOlution* 7, 1 (aug 2014), 11–23. <https://doi.org/10.1145/2661735.2661737>

Sung-Jin Chung. 1989. NP-completeness of the linear complementarity problem. *Journal of optimization theory and applications* 60 (1989), 393–399.

Eulalie Coevoet, Adrien Escande, and Christian Duriez. 2017. Optimization-Based Inverse Model of Soft Robots With Contact Handling. *IEEE Robotics and Automation Letters* 2, 3 (2017), 1413–1419. <https://doi.org/10.1109/LRA.2017.2669367>

Michael F Cohen. 1992. Interactive spacetime control for animation. In *Proceedings of the 19th annual conference on Computer graphics and interactive techniques*. 293–302.

George Corliss, Christèle Faure, Andreas Griewank, Laurent Hascoët, and Uwe Naumann. 2013. *Automatic differentiation of algorithms: from simulation to optimization*. Springer Science & Business Media.

Stelian Coros, Sebastian Martin, Bernhard Thomaszewski, Christian Schumacher, Robert Sumner, and Markus Gross. 2012. Deformable objects alive! *ACM Transactions on Graphics (TOG)* 31, 4 (2012), 1–9.

Richard W Cottle, Jong-Shi Pang, and Richard E Stone. 2009. *The linear complementarity problem*. SIAM.

Cosimo Della Santina, Christian Duriez, and Daniela Rus. 2023. Model-Based Control of Soft Robots: A Survey of the State of the Art and Open Challenges. *IEEE Control Systems Magazine* 43, 3 (2023), 30–65. <https://doi.org/10.1109/MCS.2023.3253419>

Tao Du, Kui Wu, Pingchuan Ma, Sébastien Wah, Andrew Spielberg, Daniela Rus, and Wojciech Matusik. 2021. Diffpd: Differentiable projective dynamics. *ACM Transactions on Graphics (TOG)* 41, 2 (2021), 1–21.

Theodore Gast, Chuyuan Fu, Chenfanfu Jiang, and Joseph Teran. 2016. Implicit-shifted symmetric QR singular value decomposition of 3×3 matrices. *Technical report* (2016).

Dan Givoli. 2021. A tutorial on the adjoint method for inverse problems. *Computer Methods in Applied Mechanics and Engineering* 380 (2021), 113810.

Andreas Griewank and Andrea Walther. 2008. *Evaluating derivatives: principles and techniques of algorithmic differentiation*. SIAM.

Eitan Grinspun, Anil N Hirani, Mathieu Desbrun, and Peter Schröder. 2003. Discrete shells. In *Proceedings of the 2003 ACM SIGGRAPH/Eurographics symposium on Computer animation*. Citeseer, 62–67.

Gaël Guennebaud, Benoît Jacob, et al. 2010. Eigen v3. <http://eigen.tuxfamily.org>.

Brian Guenter. 2007. Efficient symbolic differentiation for graphics applications. In *ACM SIGGRAPH 2007 papers*. 108–es.

Robert Hecht-Nielsen. 1992. Theory of the backpropagation neural network. In *Neural networks for perception*. Elsevier, 65–93.

Yuanming Hu, Luke Anderson, Tzu-Mao Li, Qi Sun, Nathan Carr, Jonathan Ragan-Kelley, and Frédéric Durand. 2019a. Diffitaichi: Differentiable programming for physical simulation. *arXiv preprint arXiv:1910.00935* (2019).

Yuanming Hu, Jiancheng Liu, Andrew Spielberg, Joshua B Tenenbaum, William T Freeman, Jiajun Wu, Daniela Rus, and Wojciech Matusik. 2019b. Chainqueen: A real-time differentiable physical simulator for soft robotics. In *2019 International conference on robotics and automation (ICRA)*. IEEE, 6265–6271.

Yixin Hu, Qingnan Zhou, Xifeng Gao, Alec Jacobson, Denis Zorin, and Daniele Panozzo. 2018. Tetrahedral meshing in the wild. *ACM Trans. Graph.* 37, 4 (2018), 60.

Zizhou Huang, Davi Colli Tozoni, Arvi Gjoka, Zachary Ferguson, Teseo Schneider, Daniele Panozzo, and Denis Zorin. 2022. Differentiable solver for time-dependent deformation problems with contact. *ACM Transactions on Graphics* (2022).



Fig. 12. **A librarian stool.** A soft robot stool carries a book, walks like a quadruped and leaves the book to slide down and stack on another book. This animation can be intuitively generated by combining several kinematic targets. Our method resolves the stool-ground contacts and stool-book contacts to allow the stool to complete this mission successfully.

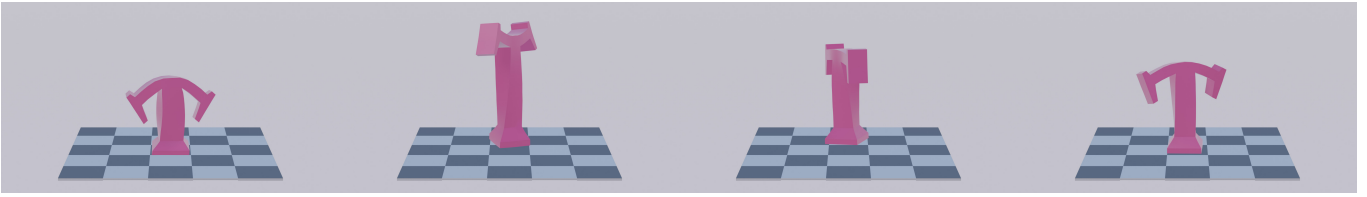


Fig. 13. **T jumps and rotates.** This is a classic locomotion example. A T-shaped body jumps, lands, and rotates. We could replicate the locomotion result of [Tan et al. 2012].

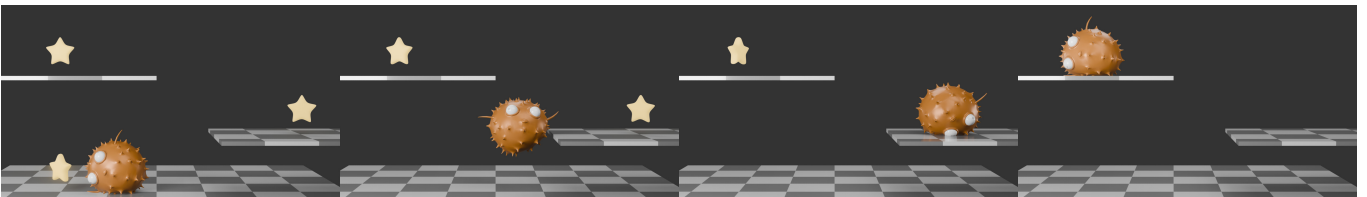


Fig. 14. **Puffer fish's playground.** The spiky puffer fish rolls and leaps between three planks, taking the stars at the target location.

Junggon Kim and Nancy S Pollard. 2011. Fast simulation of skeleton-driven deformable body characters. *ACM Transactions on Graphics (TOG)* 30, 5 (2011), 1–19.

Sanghaun Kim, Junghyun Ryu, and Maenghyo Cho. 2011. Numerically generated tangent stiffness matrices using the complex variable derivative method for nonlinear structural analysis. *Computer Methods in Applied Mechanics and Engineering* 200, 1–4 (2011), 403–413.

Minchen Li, Zachary Ferguson, Teseo Schneider, Timothy Langlois, Denis Zorin, Daniele Panozzo, Chenfanfu Jiang, and Danny M. Kaufman. 2020. Incremental Potential Contact: Intersection-and Inversion-Free, Large-Deformation Dynamics. *ACM Transactions on Graphics* 39, 4 (Aug. 2020), 49:49:1–49:49:20. <https://doi.org/10.1145/3386569.3392425>

Chen Liang, Xifeng Gao, Kui Wu, and Zherong Pan. 2023. Learning Reduced-Order Soft Robot Controller. *arXiv:2311.01720* [cs.RO]

C Karen Liu, Aaron Hertzmann, and Zoran Popović. 2005. Learning physics-based motion style with nonlinear inverse optimization. *ACM Transactions on Graphics (TOG)* 24, 3 (2005), 1071–1081.

Ran Luo, Weiwei Xu, Tianjia Shao, Hongyi Xu, and Yin Yang. 2019. Accelerated complex-step finite difference for expedient deformable simulation. *ACM Transactions on Graphics (TOG)* 38, 6 (2019), 1–16.

James N Lyness. 1967. Numerical algorithms based on the theory of complex variable. In *Proceedings of the 1967 22nd national conference*. 125–133.

Charles C Margossian. 2019. A review of automatic differentiation and its efficient implementation. *Wiley interdisciplinary reviews: data mining and knowledge discovery* 9, 4 (2019), e1305.

Sehee Min, Jungdam Won, Seunghwan Lee, Jungnam Park, and Jehee Lee. 2019. Softcon: Simulation and control of soft-bodied animals with biomimetic actuators. *ACM Transactions on Graphics (TOG)* 38, 6 (2019), 1–12.

Arturo Montoya, Randal Fielder, Armando Gomez-Farias, and Harry Millwater. 2015. Finite-element sensitivity for plasticity using complex variable methods. *Journal of Engineering Mechanics* 141, 2 (2015), 04014118.

Igor Mordatch and Emo Todorov. 2014. Combining the benefits of function approximation and trajectory optimization.. In *Robotics: Science and Systems*, Vol. 4. 23.

Jorge J Moré. 2006. The Levenberg-Marquardt algorithm: implementation and theory. In *Numerical analysis: proceedings of the biennial Conference held at Dundee, June 28–July 1, 1977*. Springer, 105–116.

Lucas Mourot, Ludovic Hoyet, François Le Clerc, François Schnitzler, and Pierre Hellier. 2022. A survey on deep learning for skeleton-based human animation. In *Computer Graphics Forum*, Vol. 41. Wiley Online Library, 122–157.

J Thomas Ngo and Joe Marks. 1993. Spacetime constraints revisited. In *Proceedings of the 20th annual conference on Computer graphics and interactive techniques*. 343–350.

Chuck Pheatw. 2008. Intel® Threading Building Blocks. *Journal of Computing Sciences in Colleges* 23, 4 (April 2008), 298.

Alla Safanova, Jessica K Hodgins, and Nancy S Pollard. 2004. Synthesizing physically realistic human motion in low-dimensional, behavior-specific spaces. *ACM Transactions on Graphics (ToG)* 23, 3 (2004), 514–521.

Pierre Schegg, Etienne Ménager, Elie Khairallah, Damien Marchal, Jérémie Dequidt, Philippe Preux, and Christian Duriez. 2022. SofaGym: An open platform for Reinforcement Learning based on Soft Robot simulations. *Soft Robotics* (2022).

Siyuan Shen, Yin Yang, Tianjia Shao, He Wang, Chenfanfu Jiang, Lei Lan, and Kun Zhou. 2021. High-Order Differentiable Autoencoder for Nonlinear Model Reduction. *ACM Transactions on Graphics* 40, 4 (July 2021), 68:1–68:15. <https://doi.org/10.1145/3450626.3459754>

Eftychios Sifakis and Jernej Barbic. 2012. FEM simulation of 3D deformable solids: a practitioner's guide to theory, discretization and model reduction. In *Acm siggraph 2012 courses*. 1–50.

Breannan Smith, Fernando De Goes, and Theodore Kim. 2018. Stable neo-hookean flesh simulation. *ACM Transactions on Graphics (TOG)* 37, 2 (2018), 1–15.

Jie Tan, Yuting Gu, Greg Turk, and C. Karen Liu. 2011. Articulated swimming creatures. In *ACM SIGGRAPH 2011 papers* (Vancouver, British Columbia, Canada) (SIGGRAPH '11). ACM, Article 58, 12 pages.

Jie Tan, Greg Turk, and C. Karen Liu. 2012. Soft Body Locomotion. *ACM Transactions on Graphics* 31, 4 (July 2012), 26:1–26:11. <https://doi.org/10.1145/2185520.2185522>

Darryl G Thelen, Frank C Anderson, and Scott L Delp. 2003. Generating dynamic simulations of movement using computed muscle control. *Journal of biomechanics*

36, 3 (2003), 321–328.

Vasileios Tzoumas, Mohammad Amin Rahimian, George J Pappas, and Ali Jadbabaie. 2015. Minimal actuator placement with bounds on control effort. *IEEE Transactions on Control of Network Systems* 3, 1 (2015), 67–78.

Andrew Witkin and Michael Kass. 1988. Spacetime constraints. *ACM Siggraph Computer Graphics* 22, 4 (1988), 159–168.

Victor Zordan, David Brown, Adriano Macchietto, and KangKang Yin. 2014. Control of rotational dynamics for ground and aerial behavior. *IEEE transactions on visualization and computer graphics* 20, 10 (2014), 1356–1366.